25th ABCM International Congress of Mechanical Engineering
October 20-25, 2019, Uberlândia, MG, Brazil

COB-2019-1148
APPLICATION OF TOPOLOGY OPTIMIZATION TO THE MICROCHANNEL COOLING OF MICROPROCESSORS HOT-SPOTS

Rodrigo Vidonscky Pinto
Flávio Augusto Sanzovo Fiorelli
Universidade de São Paulo. Departamento de Engenharia Mecânica da Escola Politécnica da USP. Av. Prof. Mello Moraes, 2231. CEP 05508-030 – São Paulo – SP
rodrigovidonscky@usp.br
fiorelli@usp.br

Abstract. *Studies using topology optimization for the construction of a microchannel heat sink geometry coupled to a microprocessor currently present several solutions regarding an optimal pressure drop along this heat sink, an optimal heat dissipation from the microprocessor, or a trade-off relation between those two solutions. However, the physical model and the simplifications adopted in these studies, such as the neglect of the convective term of the Navier-Stokes equations and the adoption of velocity profiles as outlet boundary conditions, are not consistent with the physical problem. Also, there are a number of recent studies that seek to obtain a heat dissipation solution for microprocessors using the least amount of energy, removing the heat produced only in the hot-spot regions. So, the present study comprises the elaboration of an improved topology optimization process for the obtainment of a microchannel heat sink geometry regarding the correction of this physical model and these simplifications, as well as the maximum heat dissipation of only the hot-spot regions. The solution of this topology optimization process resulted in geometries clearly exposing the influence of each of these applied corrections, such as different shape transitions, asymmetrical behavior, the suppression of an outlet region and a geometry presenting a trade-off relation between minimal pressure drop and heat dissipation only in the hot spot regions.*

Keywords: *Microprocessor. Hot-spot. Topology Optimization.*

1. INTRODUCTION

The adoption of local cooling solutions for dissipating the heat emitted in the hot-spot regions of microprocessors is being recently developed in an effort to obtain a performance enhancement of the processor coupled with low energy consumption. According to Bar Cohen and Wang (2009), an effective localized cooling of the hot-spots of a microprocessor can result in a speed gain as large as 200% in some CMOS microprocessors.

Also, the existing cooling solutions applied to a microprocessor are being continuously optimized by several recent studies seeking to obtain optimal design parameters for each researched cooling technique, and consequently, consuming the least energy as possible. Examples of these optimization studies include techniques for optimally positioning micrometric sized coolers along the hot-spots of the microprocessor, such as Nain et al. (2010), techniques for the construction of heat sinks with optimized geometry, such as Koga *et al.* (2013), as well as several other heat dissipation techniques.

Specifically, the studies of Koga *et al.* (2013), De Lima *et al.* (2010) and Koga (2010) seek to use topology optimization to obtain a heat sink containing an optimal geometry of microchannels in its structure in order to dissipate the heat produced by a uniformly distributed heat source.

Although these studies succeed in providing a viable geometry for this goal, it must be stated that the problem of the cooling of a microprocessor using fluid flow across microchannels requires some different considerations than those adopted in these studies.

The first consideration regards the fluid flow motion conservation model adopted by the author. This model, based on the Stokes equations, regards the modeling of the motion conservation of a fluid flow by neglecting the convection term present in the Navier-Stokes equations, such that the steady state motion conservation equation is reduced from the Navier-Stokes form:

$$\rho\left(u\cdot\nabla\right)u=-\nabla p+\mu\nabla^2 u+f \tag{1}$$

To the Stokes form:

$$0 = -\nabla p + \mu \nabla^2 u + f \tag{2}$$

The Stokes equations can consistently predict the motion conservation for flow configurations with very low Reynolds numbers (such as 1 or smaller). This range of properties frequently is not sufficient to predict the flow characteristics in channels with micrometric dimensions, so that the full form of the Navier-Stokes equations is required for predicting the fluid flow for this application instead of the Stokes equations, as observed in Olesen et al. (2005).

The second consideration regards the boundary conditions used for representing the outlet conditions for the fluid flow along the microchannels. The study of Koga *et al.* (2013), based in Borrvall and Petersson (2003), adopted this condition as defined by a completely developed velocity profile. This is not physically accurate, since the optimization process could result in non-straight channels, and can lead the topology optimization process to alternate solutions.

The third consideration regards the aforementioned local cooling of the hot-spot regions. The use of a uniformly distributed heat source along the optimization domain as a boundary condition for the optimization problem causes the geometry evaluated by the topology optimization process to fill almost the entire domain of the heat sink. This provides solutions to the topology optimization such as the solution presented in Fig. 1, extracted from Koga *et al.* (2013).

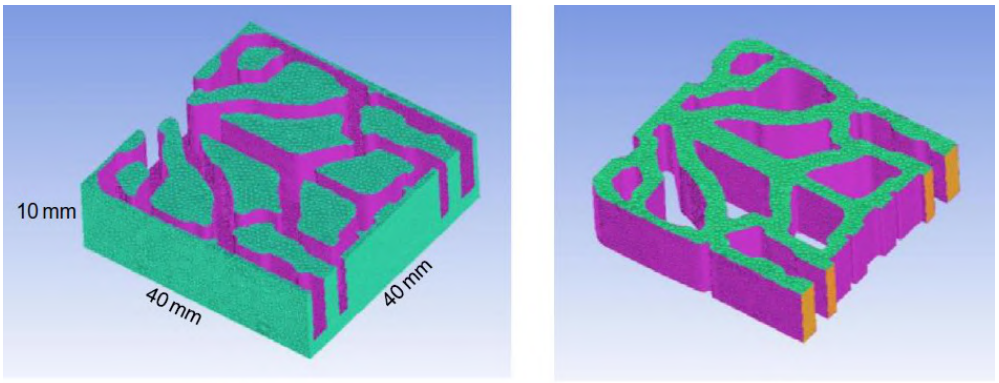

Figure 1. Microchannel geometry obtained by Koga *et al.* (2013) through topology optimization (a) solid domain (b) fluid domain

As a direct consequence, the pressure drop of this solution must be significantly higher than a solution regarding only the cooling of the hot-spot regions. Also, this solution is symmetric, completely disregarding the existence of asymmetrical heat source distributions along the microprocessor, which can be observed in multicore processors, such as the IBM dual-core PowerPC^{TM}970MP from the studies of Hamann *et al.* (2006), presented in Fig. 2.

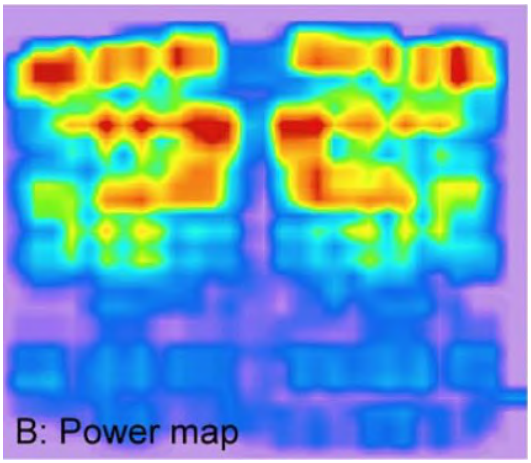

Figure 2. Power map of a IBM dual-core PowerPC^{TM}970MP (Hamann *et al.*, 2006)

So, the purpose of the present study comprises obtaining solutions for test topology optimization problems containing theoretical boundary conditions such as different fluid velocity distributions and different heat source distributions simulating real microprocessors and incorporating:

- the use of the Navier-Stokes equations for the motion conservation;
- the use of alternate boundary conditions for the flow outlet;
- the use of modified heat sources distributions containing only asymmetrical hot-spots.

2. THEORY

2.1 Finite Element Method

In order to evaluate the physical phenomena involved in the fluid flow and the heat transfer problem associated to the liquid cooling of a heat source resulting from the operation of a microprocessor through the use of microchannels, it is necessary to discretize the domain (defined as Ω) containing these microchannels into smaller domains to reduce the differential equations into a system of linear equations. Also, considering that this discretization is also used in the topology optimization process, the most suitable method regarding precision and computational cost is the Finite Element Method (FEM).

Initially, it is necessary to define the discretization scheme adopted for the creation of the nodes and the elements used in the FEM. The shape of these elements are defined for the present study as the same shape used in Koga (2010), which is quadrilateral with isoparametrical elements. This is justified in order to keep using local coordinates along the elements to simplify the calculations, as well as maintain a direct base of comparison with the literature.

These quadrilateral elements also follow the discretization scheme adopted in Koga (2010), using four nodes both for the velocity components (with two degrees of freedom each) and the temperature components (with one degree of freedom each) distributed along the vertexes of the quadrilateral element, and one node for the pressure components positioned in the center of the element. A visual representation of this discretization method can be observed in Fig. 3.

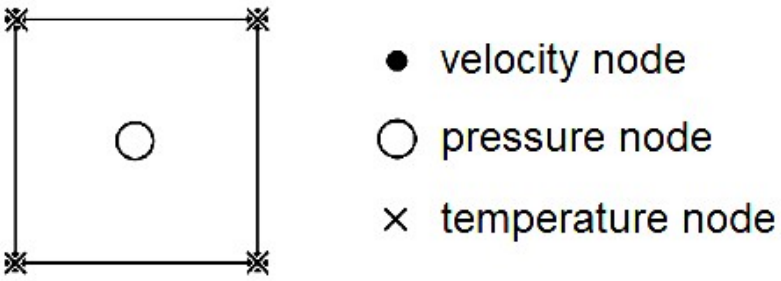

Figure 3. Discretization scheme

The hydrodynamic part (velocities and pressure) of this discretization method is commonly regarded as Q_1-P_0 (Donea and Huerta, 2003; Elman *et al.*, 2007) and usually leads to instabilities regarding the application of the Galerkin method for constructing the equations of the FEM. These instabilities are generally evaluated using the Ladyzhenskaya-Babushka-Brezzi (LBB) conditions, which are broadly known to not be satisfied using the Q_1-P_0 discretization (Donea and Huerta, 2003).

However, as described in Koga (2010), these instabilities are mainly associated with the pressure field, while the velocity field, which is the object of interest in the topology optimization, remains unchanged even using the Q_1-P_0 discretization. Also, this discretization method results in a much smaller computational cost once it uses fewer nodes than most other methods. So, the present study also remains using the Q_1-P_0 discretization method.

The hydrodynamic model presented in Koga (2010) consists in the use of the FEM in order to define an approximate solution for the weak formulation of the fluid flow along the microchannel heat sink using the conjunction of the Stokes equation with the Darcy's law. This result in the Brinkman equation, which introduces a permeability term containing an inverse permeability α to the Stokes equation:

$$0 = -\nabla p + \mu \nabla^2 u + \alpha u + f \tag{3}$$

The weak formulation can be obtained using the method of Mean Weighted Residuals (MWR). Equation (3) can be rewritten using an arbitrary coefficient v such that:

$$0 = -\int_{\Omega} p(\nabla \cdot v)\, d\Omega + \mu \int_{\Omega} \nabla u \cdot \nabla v \, d\Omega + \int_{\Omega} \alpha (u \cdot v)\, d\Omega + \int_{\Omega} f \cdot v \, d\Omega \tag{4}$$

The same can be applied to the continuity equation, using an arbitrary coefficient q such that:

$$\nabla \cdot u = 0 \tag{5}$$

Results in:

$$\int_{\Omega} q\left(\nabla \cdot u\right) d\Omega = 0 \tag{6}$$

So, considering the adoption of approximate solutions, Eqs. (4) and (6) can be rewritten such that:

$$0 = -\int_{\Omega} p\left(\nabla \cdot \tilde{v}\right) d\Omega + \mu \int_{\Omega} \nabla \tilde{u} \cdot \nabla \tilde{v}\, d\Omega + \int_{\Omega} \alpha\left(\tilde{u} \cdot \tilde{v}\right) d\Omega + \int_{\Omega} f \cdot \tilde{v}\, d\Omega \tag{7}$$

$$\int_{\Omega} q\left(\nabla \cdot \tilde{u}\right) d\Omega = 0 \tag{8}$$

The application of the Galerkin formulation reduces the approximate solutions for single generic elements using weighting functions as coefficients of the nodal variables:

$$\tilde{u} = N_u{}^T U_i \tag{9}$$

$$\tilde{p} = N_p{}^T P_i \tag{10}$$

So, the application of Eqs. (9) and (10) to the system of Eqs. (7) and (8) result in a reduced matrix form for a single generic element such as:

$$\begin{bmatrix} \mu \int_{\Omega_e} \nabla N_u \cdot \nabla N_u\, d\Omega + \int_{\Omega_e} \alpha N_u N_u\, d\Omega & -\int_{\Omega_e} N_p{}^T \left(\nabla \cdot N_u\right) d\Omega \\ \int_{\Omega_e} \left(\nabla N_u\right)^T N_p\, d\Omega & 0 \end{bmatrix} \begin{Bmatrix} U \\ P \end{Bmatrix} = \begin{Bmatrix} \int_{\Omega_e} \left(N_u\right)^T f\, d\Omega \\ 0 \end{Bmatrix} \tag{11}$$

Or, in a simplified way:

$$\left[K_e\right]\left\{X_e\right\} = \left\{F_e\right\} \tag{12}$$

Where K_e comprehends the stiffness matrix for any single element, X_e is the vector containing the velocities and pressure fields along this element and F_e assemble the motion source terms and zero elements to satisfy the continuity equation.

The assemble of Eq. (12) for each element through the whole domain result in the global equation:

$$\left[K_g\right]\left\{X_g\right\} = \left\{F_g\right\} \tag{13}$$

The heat transfer problem of a two dimensional steady state flow with heat source terms can be described using the simplified thermal energy conservation equation defined in Incropera *et al.* (2007) such as:

$$\rho c_p \left(u \cdot \nabla T\right) + f_T = k \nabla^2 T \tag{14}$$

This equation comprises a convective term containing the velocity of the fluid, a heat source term and a diffusive term containing the thermal conductivity. Once again, the MWR method can be applied in order to obtain the weak formulation of this equation. So, considering the adoption of approximate solutions for the temperature, Eq. (14) can be rewritten such as:

$$\int_V \tilde{T}\left[\rho c_p \left(u\cdot\nabla T\right)^T\right] dV + \int_V \tilde{T}\left[\nabla\cdot\left(k\nabla T\right)\right] dV = \int_V \tilde{T} Q dV \tag{15}$$

Such that this approximate solution can also be reduced using the Petrov-Galerkin formulation in order to prevent the formation of instabilities resulting from the convective term along the numerical solution of the problem. According to Koga (2010), the Petrov-Galerkin formulation differs from the traditional Galerkin formulation by the introduction of a stabilizer function, such that the weighting function w_{pg} of the Petrov-Galerkin formulation becomes the sum of the weighting function of the traditional Galerkin method w_g with this stabilizer function w_e such that:

$$w_{pg} = w_g + w_e \tag{16}$$

This stabilizer function is provided for a single generic element in Zinkiewicz and Taylor (2002) as a function of the Péclet number such as:

$$w_e = \left(\coth Pe - \frac{1}{Pe}\right)\frac{h}{2}\frac{u_e \nabla w_g}{|u_e|} \tag{17}$$

Such that h is the mean length of the single element.
So, using the Petrov-Galerkin formulation, the approximate solution for a single generic element becomes:

$$\tilde{T} = {w_{pg}}^T T_i \tag{18}$$

Obtaining from Eq. (15) that, for any single generic element:

$$\left[\int_{V_e} w_{pg}\left[\rho c_p \left(N_u u\right)^T \nabla w_g\right] dV_e + \int_{V_e} \left(\nabla w_g\right)^T \left(k\nabla w_g\right)^T dV_e\right]\{T\} = \left\{\int_{V_e} {w_g}^T Q dV_e\right\} \tag{19}$$

Or, in a simplified way:

$$\left[K_{T,e}\right]\{T_e\} = \{F_{T,e}\} \tag{20}$$

Where $K_{T,e}$ comprehends the thermal stiffness matrix for any single element, T_e is the vector containing the temperatures along this element and $F_{T,e}$ assemble the heat source terms.
The assemble of Eq. (20) for each element through the whole domain result in the global thermal equation:

$$\left[K_{T,g}\right]\{T_g\} = \{F_{T,g}\} \tag{21}$$

2.2 Topology Optimization

In order to perform a topology optimization along the microchannel heat sink domain, it is necessary to represent mathematically the variation of the properties of the materials contained in this domain, associating each element of the discretized domain with a solid used to bound the microchannels, a fluid responsible for dissipating the heat provided by the microprocessor or a porous domain coupling both of these materials. This model is represented as a material model in which each element along the domain is assigned with a discrete value representing the kind of material contained in this domain.

In this study, in agreement with the model used in Koga (2010), the material model is defined using the density method (Bendsøe, 1989), also known as SIMP (Solid Isotropic Material with Penalization). This model defines that each property of the material can be written as a function of a pseudodensity ψ which varies between 0 (for a pure solid material) and 1 (for a pure fluid material), such that each material property is modeled as a continuous function presenting a distribution of values between the properties of the two materials involved in the construction of this model.

This converts the discrete problem associated to the geometry of the microchannels in a continuous problem. However, according to Koga (2010), this conversion allows the pseudodensity ψ to assume intermediate values (herein

referred as gray scales), which must be eliminated of the final solution in order to result in a desired continuous and nonporous structure.

This pseudodensity is used to construct a function to define the behavior of an inverse permeability α, required for the solution of the Brinkman equation (Eq. 4). This function consists in:

$$\alpha = \alpha_U + \left(\alpha_L - \alpha_U\right)\psi \frac{1+q}{\psi+q} \tag{22}$$

Where α_U and α_L are the upper and the lower limits of the inverse permeability and q is a penalty factor responsible for discretizing the inverse permeability distribution.

Also, the same pseudodensity is used to construct linear weighting functions in order to define the behavior of the physical properties requires for the solution of the thermal energy conservation equation (Eq. 14). These functions can be defined for a pair of materials defined as A and B such as:

$$\rho = \psi\rho_A + \left(1-\psi\right)\rho_B \tag{23}$$

$$c_p = \psi c_{p,A} + \left(1-\psi\right)c_{p,B} \tag{24}$$

$$k = \psi k_A + \left(1-\psi\right)k_B \tag{25}$$

The work of Koga (2010) also adopted an additional penalty factor p to the material model in order to make the relation between the pseudodensity and the distribution of the properties values closer to discrete function for further iterations. However, in the present study, it is very important to ensure that the fluid regions that assure the continuity of the flow remain unobstructed along the optimization process in order to obtain convergence in the solution of the Navier-Stokes problem. This required that the penalty factor remained fixed as 1 along all the optimization process.

So, to remove the gray areas formed along the optimization process, the pseudodensity distribution ψ was subject to an extremization process after every 50 iterations, which stabilize the convergence process to a discrete solution, overcoming many local minima that could appear due the formation of the gray scale. This extremization may require a posterior smoothing of the pseudodensity distribution ψ to compensate the formation of "peninsular elements" in some studied configurations, but result in stable and converged solutions.

2.3 Numerical procedures

The solution of the fluid flow and heat transfer problem is based in the numerical integration using Gauss-Legendre method for Eqs. (14) and (21), resulting in local matrixes which, once assembled in the global matrixes, can provide the solution for the velocities, pressures and temperatures fields for the whole domain using any linear solver.

So, once the velocities, pressures and temperatures fields are obtained, it is necessary to define two important aspects for performing a topology optimization analysis: the optimization problem, composed by an objective function and the constraints of the optimization domain; and the numerical solver best suited for the solution of this optimization problem.

The objective function related to the problem of construction of a microchannel geometry for fluid flow must enclose two main physical considerations: the optimized solution must present a combination of a minimal pressure drop resulting from the fluid flowing along the microchannel structure and a maximum heat dissipation resulting from the heat transfer occurring between the microprocessor (represented as a heat source distribution) and the fluid. Each of these considerations can be represented by a different objective function, directly dependent on the parameters obtained from the solution of the conservation equations.

For the pressure drop, according to Bendsøe and Sigmund (2004), the minimization of the pressure drop corresponds to the minimization of the energy dissipation in the system. This corresponds to maximizing the "flow compliance", minimizing so the mean pressure drop along the whole domain.

According to Koga (2010), this corresponds to the minimization of an objective function defined as:

$$\Phi = \left\{X_g\right\}^T \left[K_g\right] \left\{X_g\right\} \tag{26}$$

In a similar manner, for the heat dissipation, according to Koga (2010), the objective function can be presented in its discretized form such as:

$$\Gamma = \left\{T_g\right\}^T \left[K_{T,g}\right]^T \left\{T_g\right\} \tag{27}$$

The combination of Eqs. (26) and (27) provide that a multiobjective function can be obtained. However, it must be noted that in order to minimize the pressure drop and maximize the heat dissipation, the multiobjective objective function must be expressed as a difference between these objective functions so that the first term is minimized and the second term is maximized. Also, these objective functions are in a completely different order of magnitude, so that a weighting factor must be associated to these functions in order to gather them in a single multiobjective objective function.

The present study defined this multiobjective objective function as:

$$\Lambda = \left(w_{pd}\Phi\right) - \left(w_{hd}\Gamma\right) \tag{28}$$

Such that w_{pd} and w_{hd} correspond to the weighting factors defined for pressure drop and heat dissipation, respectively. The present study adopts the values of 1 and 10^{-20} for w_{pd} and w_{hd}, respectively.

As for the constraints, there are two major constraints adopted in this study for this optimization problem.

The first constraint is given by the conservation equations. These equations provide equality constraints, since each solution must necessarily satisfy those equations in order to validate the physical phenomena occurring along the flow through the microchannels. So, Eqs. (13) and (21) are defined as constraints to this optimization process.

The second constraint comprehends the values admitted for the pseudodensities ψ along the optimization domain. These values must remain between 0 and 1 to respect the adopted material model. So, this constraint is defined as:

$$\left\{0\right\} \leq \left\{\psi\right\} \leq \left\{1\right\} \tag{29}$$

The linear nature observed for the objective function and the constraints indicates that this problem is suitable for a solution using linear programming techniques. Along those techniques, Koga (2010) explains that, since this optimization problem involves a large number of variables and constraints, the use of the method of Sequential Linear Programming (SLP) is considered reliable, and so this method is also used in the present study.

The procedure of SLP consists in expanding both the objective function and the constraints of an optimization problem into a truncated Taylor series, obtaining a optimization sub problem that consists in a new objective function defined as the gradient of the original objective function, constrained by mobile boundaries for this sub problem in order to assure that the approximation provided by this series expansion is valid into these boundaries. Figure 4, extracted and adapted from Koga (2010), provides a one-dimensional example of this method, showing that the minimization of the gradient (herein represented as a derivative) corresponds to the minimization of the objective function if the mobile boundaries are correctly imposed.

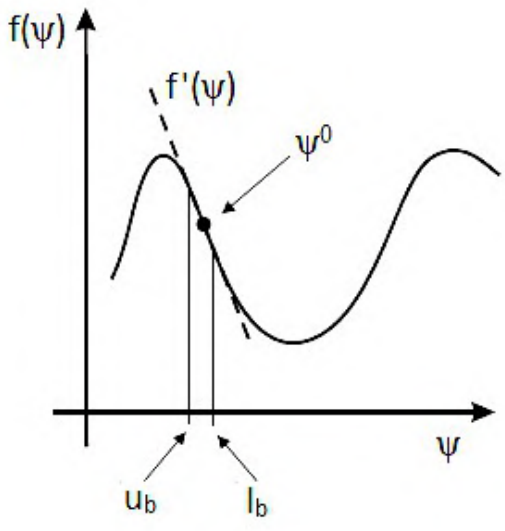

Figure 4. SLP one-dimensional representation, extracted and adapted from Koga (2010)

So, the application of SLP to the optimization process requires the definition of two parameters: The gradient of each objective function in function of the pseudodensity ψ and the range of validity defined for the mobile boundaries.

The gradient of the pressure drop objective function (Eq. 26) is defined by Koga (2010) as:

$$\frac{d\Phi}{d\psi_i} = \frac{1}{2}\{X\}^T \left[\frac{dK_g}{d\psi_i}\right]\{X\} + \{X\}^T \left[K_g\right]\left\{\frac{dX}{d\psi_i}\right\} \tag{30}$$

And the gradient of the heat transfer objective function (Eq. 27) is defined by Koga (2010) as:

$$\frac{d\Gamma}{d\psi_i} = \left\{\frac{dT_g}{d\psi_i}\right\}^T \left[K_{T,g}\right]^T \{T_g\} + \{T_g\}^T \left[\frac{dK_{T,g}}{d\psi_i}\right]^T \{T_g\} + \{T_g\}^T \left[K_{T,g}\right]^T \left\{\frac{dT_g}{d\psi_i}\right\} \tag{31}$$

The definition of each partial derivative is discussed in detail in Koga (2010).

As for the mobile boundaries, both the upper and the lower boundaries are set for the five first iterations as half of the value defined for each pseudodensity ψ, but respecting the boundaries defined by the pseudodensity constraint (Eq. 29). As the iterations progress and the geometry of the channel become closer of the final geometry, they are reduced gradually to 1/3 of the value defined for each pseudodensity.

3. ANALYSIS

The contribution of the present study to the model used for the construction of the topology optimization algorithm is divided in two main aspects in this section: a hydrodynamic aspect, referring to the adoption of the corrections to the Stokes equation in order to obtain a valid Navier-Stokes solution and to the correction of the outlet boundary condition, and a thermal aspect, referring to the modification of the heat source used for obtaining the gradients used in the heat transfer optimization process in order to emphasize the heat dissipation along the hot-spots.

3.1 Hydrodynamic

Initially, it must be stated that while the Brinkman equation is a linear differential equation and can be easily solved using usual numeric methods such as the Finite Element Method (FEM) or the Finite Differences Method (FDM), the Navier-Stokes equation is a nonlinear differential equation, once that first term of this equation (the convection term) has coefficients that also depend on the velocities along the domain to produce a solution. This requires an iterative process in which an initial velocity is estimated using a considerably good guess and repeatedly recalculated until a minimal residual is achieved between two consecutive solutions.

An approach currently defined as suitable for this iterative process and commonly used in consolidated algorithms along the literature (such as Liu *et al.*, 2015 and Sylvester *et al.*, 2019) consists in linearizing the convection term of the Navier-Stokes equation using the Picard method. This method reduces the nonlinear Navier-Stokes equations to a form known as the Oseen equation:

$$\rho\left(\boldsymbol{u}_{k-1}\cdot\nabla\right)\boldsymbol{u}_k = -\nabla\boldsymbol{p}_k + \mu\nabla^2\boldsymbol{u}_k + \boldsymbol{f} \tag{32}$$

So, according to Ur Rehman *et al.* (2008), once there is an initial guess for the velocity field, it can be used for estimating the velocity present in the coefficient used in the subsequent iteration and so on.

This linearization results in a saddle point problem, which in most complicated cases requires the use of conditioning techniques in order to achieve a consistent solution, such as the use of conditioning stabilizing elements (Sylvester *et al.*, 2019) or factorization techniques (Ur Rehman *et al.*, 2008). These techniques are not necessary for the solution of the example problems of the present study, so they are not discussed in detail.

So, all that remains consists in defining the initial guess for the iterative process. Sylvester *et al.* (2019) and Liu *et al.* (2015) defined this initial guess as the solution of the Stokes flow, since this flow is considerably similar to the actual Navier-Stokes flow when the velocities are very small. So, since the use of microchannels limit these velocities to small values, this initial guess is considered suitable for the present study and used therefore.

As for the outlet boundary condition, there are some conditions commonly adopted along the literature regarding the use of computational fluid dynamics (CFD) that represent this exit condition more correctly than a developed velocity profile. These conditions include the adoption of a zero-gradient region (Versteeg and Malakasera, 2007), a zero relative pressure region for incompressible flows with constant density and no backflow at the outlet (Bakker and Marshall, 2004), among other conditions.

So, in accordance to the literature, after the initial validation tests, the outlet boundary condition is defined as a pressure boundary condition and adopted thereafter.

3.2 Thermal

From a thermal perspective, it can be observed that the thermal energy conservation equation depends on the motion conservation equations since there is a convective term in which there is the presence of the velocity variable. This could lead to the need of coupling the solution of the conservation equations in order to satisfy both equations simultaneously. However, due to the small velocities found in microchannels, these equations were solved without coupling in the present study.

Also, once the heat provided by a microprocessor to the flow is represented the a heat source term, and since there is no initial difference of temperature between the microprocessor and the flow, the propagation of the heat provided by this source term to the fluid flow performed by the fluid motion provides the major contribution for the formation of the temperature gradients along the flow and for the geometry obtained through topology optimization. This means that even small heat source terms evenly distributed along the domain may affect the obtained geometry resulting in a greater pressure drop.

So, the present study seeks to provide microchannel structures that neglect all the heat source terms that are not located in the hot-spot regions of the microprocessor.

To achieve this objective, the source terms are filtered in order to extract a number of heat sources presenting the highest values along the heat source distribution and insert these heat sources in a clear heat source distribution. Also, all the heat sources surrounding these hot spots are also inserted in this new distribution, in order to enclose all elements under influence of these hot-spots This results in new heat source distribution containing only these heat sources, which can be applied to the topology optimization algorithm, resulting in optimization gradients that lead to a very different solution than the solution obtained using the complete heat source.

4. METHODOLOGY

The process of obtaining an optimal solution for the geometry of the microchannels used for dissipating the heat produced by a theoretical heat source using topology optimization can be represented as the iterative process described by the flowchart presented in Fig. 5.

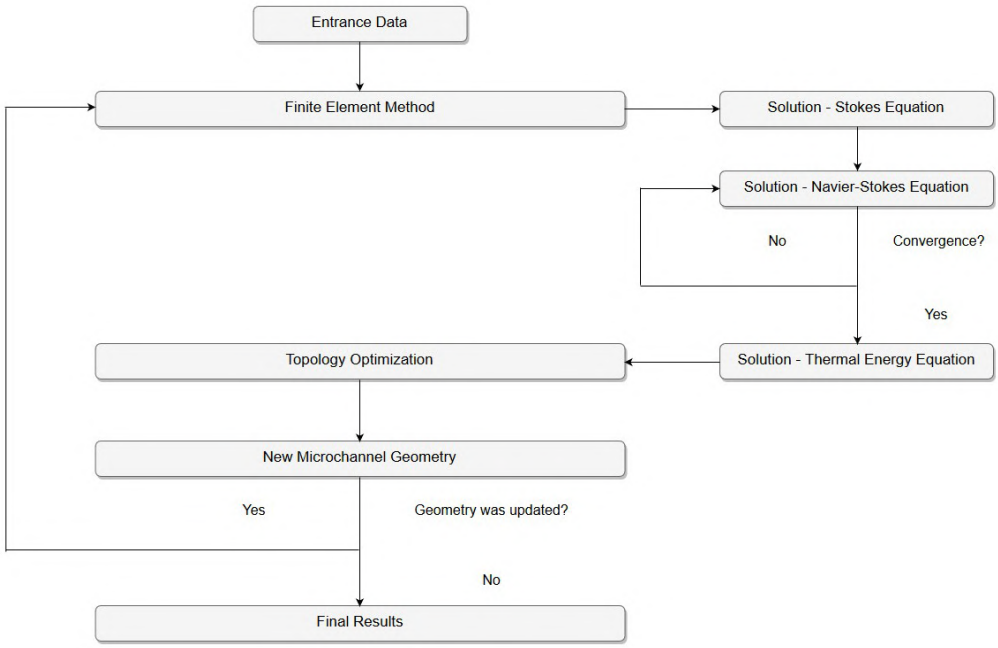

Figure 5. Methodology flowchart

So, it becomes necessary to define a geometry convergence condition in order to produce a final solution. This condition is defined as the difference between the geometry obtained between two extremization processes (executed after every 50 iterations). If the pseudodensity of any element of the domain is changed between two subsequent

extremization processes, the iterative process executes 50 additional iterations in order to perform the next comparison. Otherwise, the algorithm provides the last extremization as the final solution.

4.1 Entrance data

In order to simulate the conditions faced by a microchannel heat sink coupled to the die of a real microprocessor, the domain of this study is defined as a flat plate with 30 mm x 20 mm and a thickness of 1.6 mm, corresponding to the thickness of a heat spreader plate located between the microprocessor die and the actual heat sink of a microprocessor (usually referred as the Integrated Heat Spreader – IHS), which could be used as the base structure for the construction of the microchannel heat sink.

This flat plate was subdivided in square elements of 0.5 mm x 0.5 mm, resulting in a 60 x 40 grid containing 61 x 41 nodes for a total of 2400 elements and 2501 nodes. Figure 6 presents a graphical representation of the constructed grid.

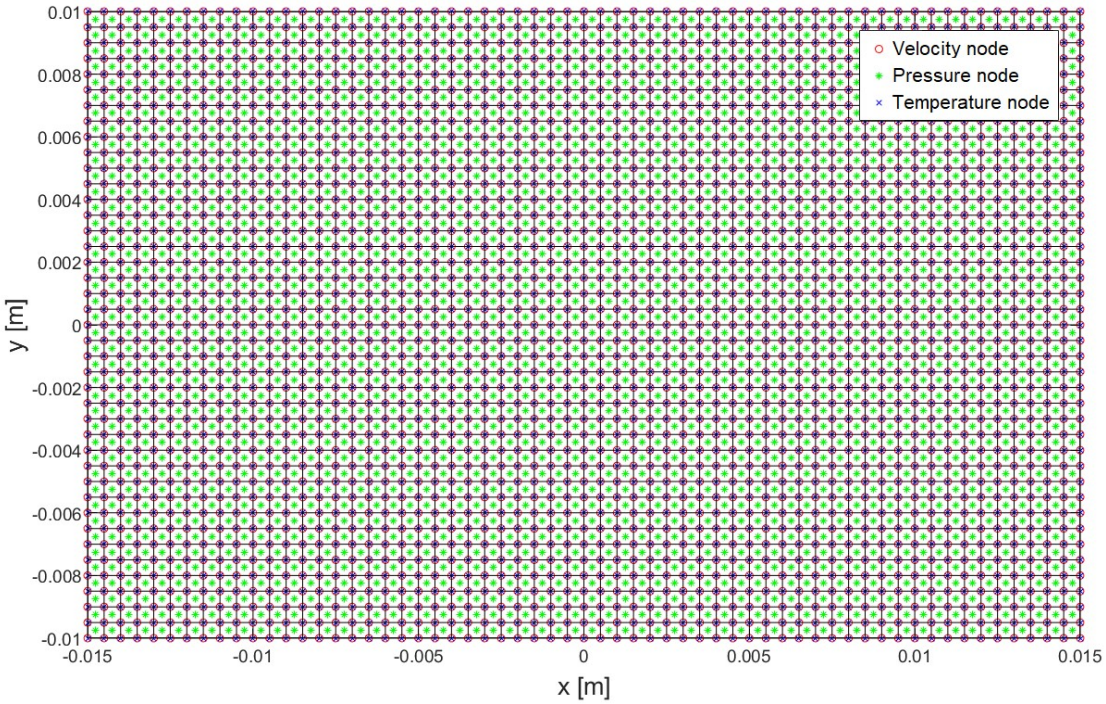

Figure 6. Microchannel domain grid

Since each node contains two degrees of freedom for the velocity in each coordinate direction, this results in velocity fields containing 5002 components for each domain. Also, since the pressure is element-centered, this results in pressure fields containing 2400 components for each domain. Finally, since each node contains a degree of freedom for the temperature and for the heat source, this results in temperature and heat source fields containing 2501 components.

Liquid water and solid copper are defined as the fluid and the solid materials, respectively. The physical properties of each of these materials (Parry, 2009; Haynes *et al.,* 2016) are considered constant and defined as their value at 20ºC, presented in Tab. 1.

Table 1. Physical properties of selected materials at 20ºC

	Water	**Copper**
ρ (kg/m³)	998.2	8960
k (W/m.K)	0.598	385
c_p (J/kg.K)	4184.8	401
μ (N.s/m²)	10^{-3}	-

As for the constants used for the definition of the inverse permeability α using Eq. (22), since the orders of magnitude of the geometrical dimensions of the present study are smaller than the order of magnitude of these dimensions in Koga (2010) and Borrvall and Petersson (2003), an adjustment to the upper and lower boundaries of the inverse permeability is necessary.

So, for the present study, these boundaries are defined as:

$$\alpha_U = \frac{2.5\mu}{0.01^4} \tag{33}$$

$$\alpha_L = \frac{2.5\mu}{100^4} \tag{34}$$

However, the penalty factor q assumed a constant value of 0.1, in agreement with the value used in Koga (2010) for latter iterations.

Finally, it is necessary to define an initial pseudodensity distribution ψ in order to obtain a preliminary flow as a starting condition. So, to assure a continuity condition, for all studied cases, the initial pseudodensity was defined as 1 for all elements, which means that, initially, the entire domain is filled with fluid elements.

4.2 Studied applications

The present study uses these geometry and these physical properties as a base to study several test configurations coupled to the formulations presented in previous chapters in order to explicit the influence of the adopted corrections.

The first test configuration consists in a double pipe channel configuration presented in Borrvall and Petersson (2003) and in Koga (2010). This configuration consists in a rectangular domain with two inlet entrances modeled as developed velocity profiles located at the left side of the domain and two output exits modeled as developed velocity profiles located at the right side of the domain. All these velocity profiles are parabolic and present a maximum velocity located at the center of each profile, and zero velocity along their borders. Also, in most of the cases, the magnitude of this maximum velocity is defined as 20 mm/s.

A graphical representation of this configuration, adapted from Koga (2010), can be observed in Fig. 7.

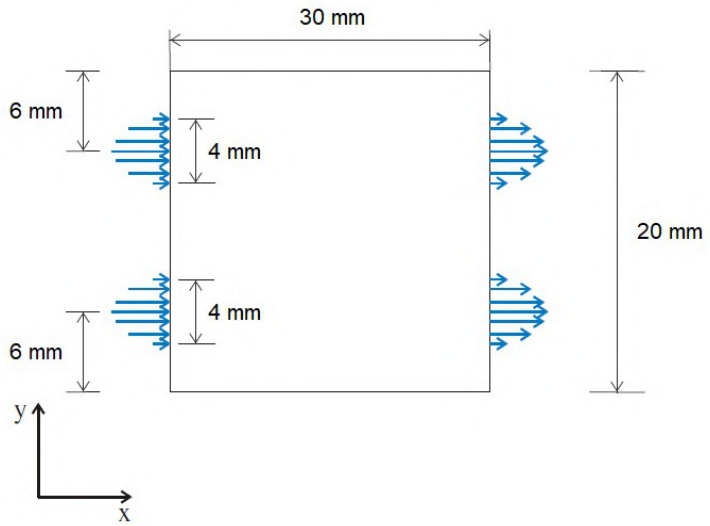

Figure 7. Double pipe channel configuration

This configuration is subject to the pressure drop topology optimization process mainly to observe the effect of two corrections.

The first correction consists in a direct comparison between the geometry obtained with the topology optimization of the pressure drop objective function using the solution of the Brinkman equation along this domain and the geometry obtained using the Navier-Stokes correction to include convective effects along this domain. Both these cases still are evaluated using the outlet boundary conditions as developed velocity profiles.

The second correction consists in comparing the geometry obtained using outlet boundary conditions as developed velocity profiles with the geometry obtained setting the relative pressure at these boundaries as zero. Both these cases are evaluated using the Navier-Stokes correction.

The second test configuration consists in a single pipe channel configuration. The hydrodynamic characteristics of this configuration comprehend the same rectangular domain used in the first configuration, now containing only one inlet entrance modeled as a developed velocity profile located at the center of left side of the domain and only one output exit modeled as a zero relative pressure region located at the center of right side of the domain. Also, all cases in this configuration are modeled using the Navier-Stokes correction.

A central portion with half the length of the domain is filled with heat source terms of 0.005 W each. Finally, two hot spots of 0.1 W each are asymmetrically positioned along the microchannel domain, in the coordinates:

$$HS_1 = (15.5\,,15.5)\,[mm] \tag{35}$$

$$HS_2 = (13.5\,,17.5)\,[mm] \tag{36}$$

A graphical representation of this configuration can be observed in Fig. 8.

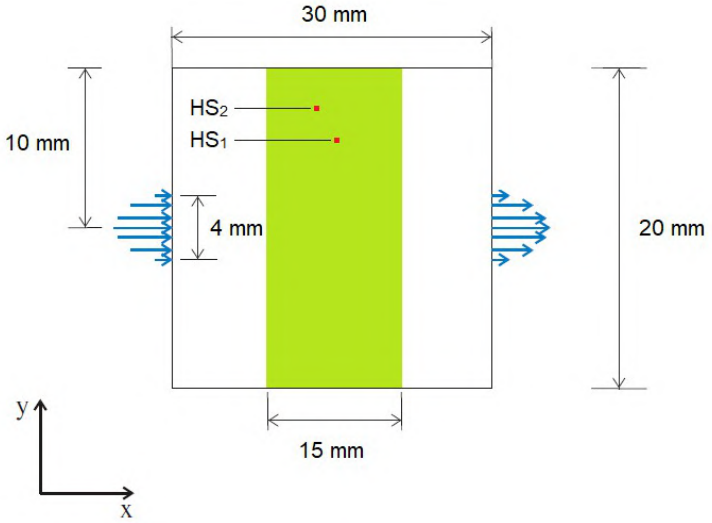

Figure 8. Single pipe channel configuration

This configuration is subject to the multiobjective topology optimization process mainly to observe the effect of the substitution of the full heat source term to an auxiliary heat source containing only the heat source terms located near the hot-spots of the heat source. This auxiliary heat source can be observed in Fig. 9.

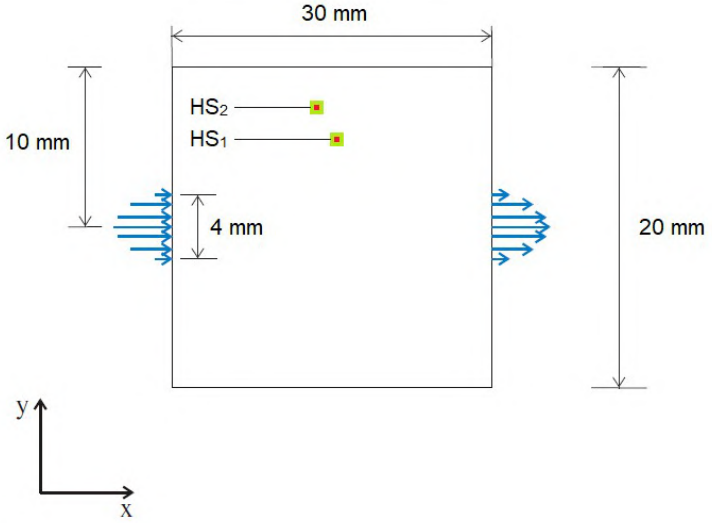

Figure 9. Single pipe channel configuration with hot-spot heat source

5. RESULTS

The microchannel geometries obtained using the topology optimization process for the first test configuration can be observed in Fig. 10 with (b) and without (a) the correction regarding the convective term of the Navier-Stokes equations.

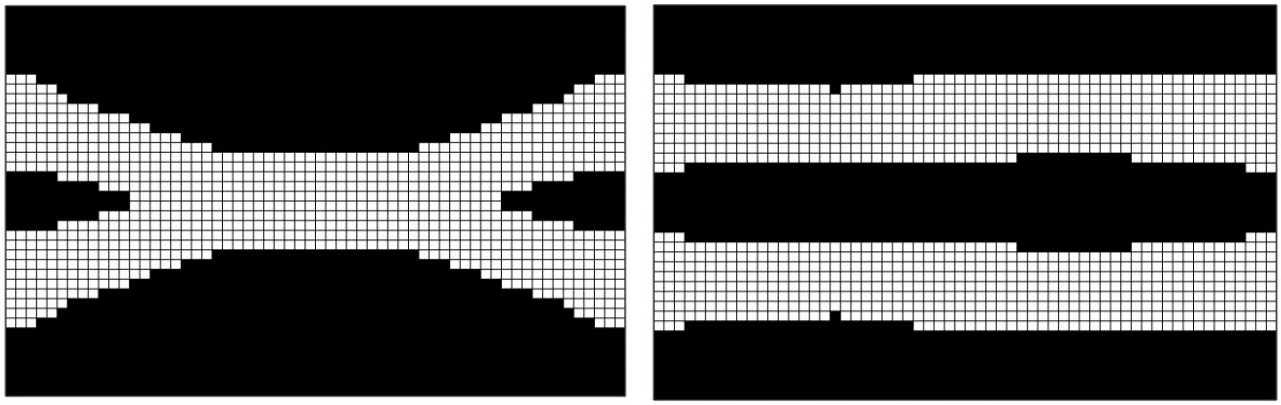

(a) (b)

Figure 10. Microchannel geometry for the microprocessor heat sink using (a) Brinkman equation (b) Navier-Stokes correction

Clearly, the adoption of the convective term influenced the shape of the microchannels, transforming a convergent-divergent symmetric single channel structure in a separated double channel structure. The adoption of the Navier-Stokes correction affects the symmetry of the convergent-divergent single channel structure observed in Fig. 10(a) due the convective effects incorporated to the fluid flow. The convergent entrance of the channel structure becomes more convergent, providing space for the divergent exit of the channel structure develop the fluid flow.

Also, it can be observed that the geometry presented Fig. 10(b) is not exactly a pair of straight channels, containing a few small disturbances. These disturbances are generated by the successive execution of the optimization algorithm permuting through a series of similar optimal solutions.

Furthermore, as observed in Borrvall and Petersson (2003) and in Koga (2010), it is still possible to observe a transition from a separated double channel structure to a convergent-divergent single channel structure using the Navier-Stokes correction when you increase the channel length or the mean inlet velocity. Figures 11(a) and 11(b) present the microchannel geometries obtained for a base geometry with 80 mm x 20 mm and for an inlet with maximum velocity of 40 mm/s, respectively.

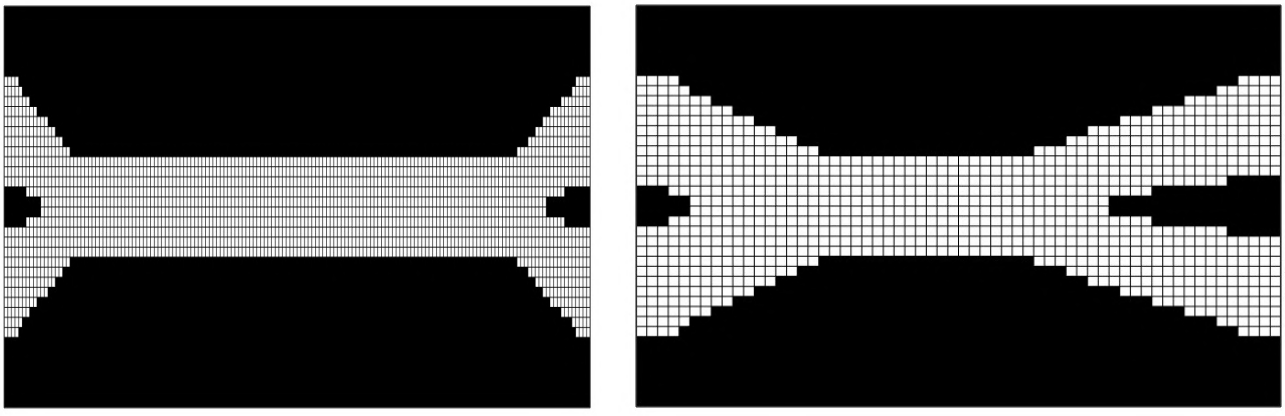

(a) (b)

Figure 11. Microchannel geometry for the microprocessor heat sink using Navier-Stokes corrections and (a) a longer channel domain (b) a higher inlet velocity

It is important to notice from Figs. 11(a) and 11(b) that the adoption of the Navier-Stokes correction affects the symmetry of the convergent-divergent single channel structure observed in Fig. 10(a) due the convective effects incorporated to the fluid flow. The convergent entrance of the channel structure becomes more convergent, providing space for the divergent exit of the channel structure develop the fluid flow. Also, it can be observed that a longer channel domain resulted in a very long unified single channel almost symmetric, while the increase in velocity resulted in a more convergent-divergent pattern.

Next, the microchannel geometries obtained using the topology optimization process for the first test configuration with the correction regarding the zero relative pressure boundary condition set to the outlets of the flow can be observed in Fig. 12 for the base entrance data and in Figs. 13(a) and 13(b) for the variants presented in Figs. 11(a) and 11(b).

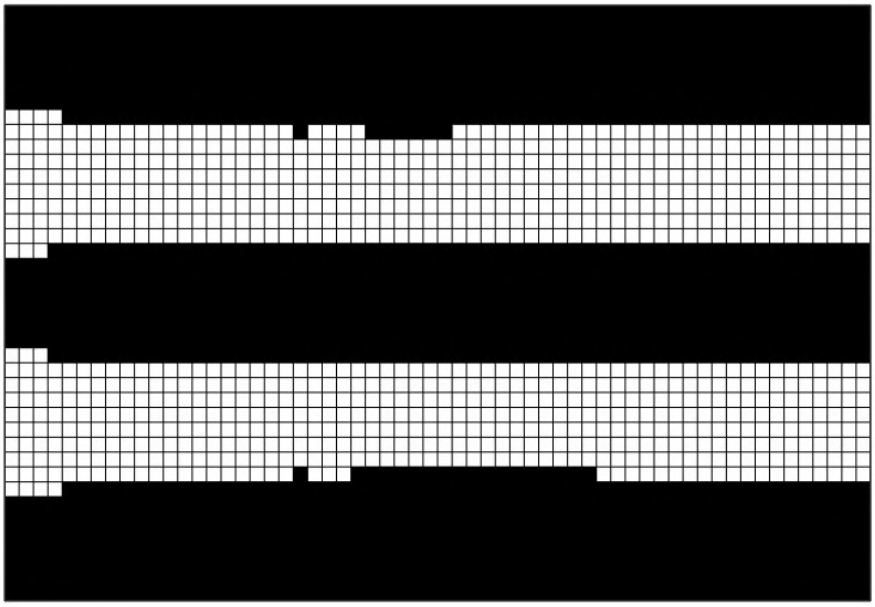

Figure 12. Microchannel geometry for the microprocessor heat sink using Navier-Stokes corrections and the zero relative pressure boundary condition

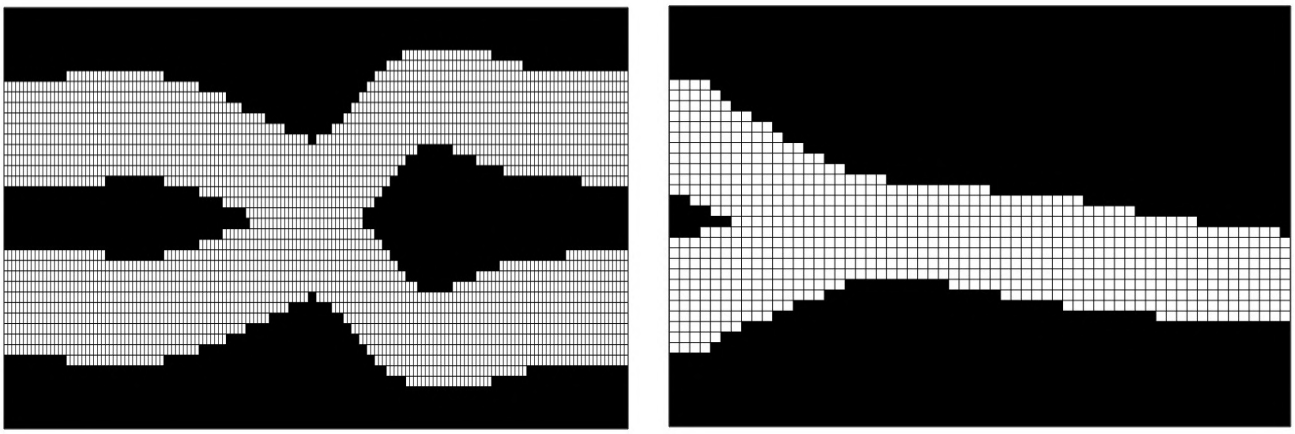

(a) (b)

Figure 13. Microchannel geometry for the microprocessor heat sink using Navier-Stokes corrections, the zero relative pressure boundary condition and (a) a longer flat plate (b) a higher inlet velocity

It is important to notice that, while the adoption of the zero relative pressure boundary condition using the base geometry as presented in Fig. 12 resulted in small differences so that this solution remained a pair of straight channels, the solution corresponding to a convergent-divergent single channel structure presented in Figs 11(a) and 11(b) is significantly modified. Fig. 13(a) presents a convergent-divergent channel with a very small single channel section, and Fig. 13(b) presents a convergent single channel structure with only one outlet section.

Finally, the microchannel geometries obtained using the topology optimization process for the second test configuration with the heat source distributions defined in Figs. 8 and 9 can be observed in Figs. 14(a) and 14(b), respectively.

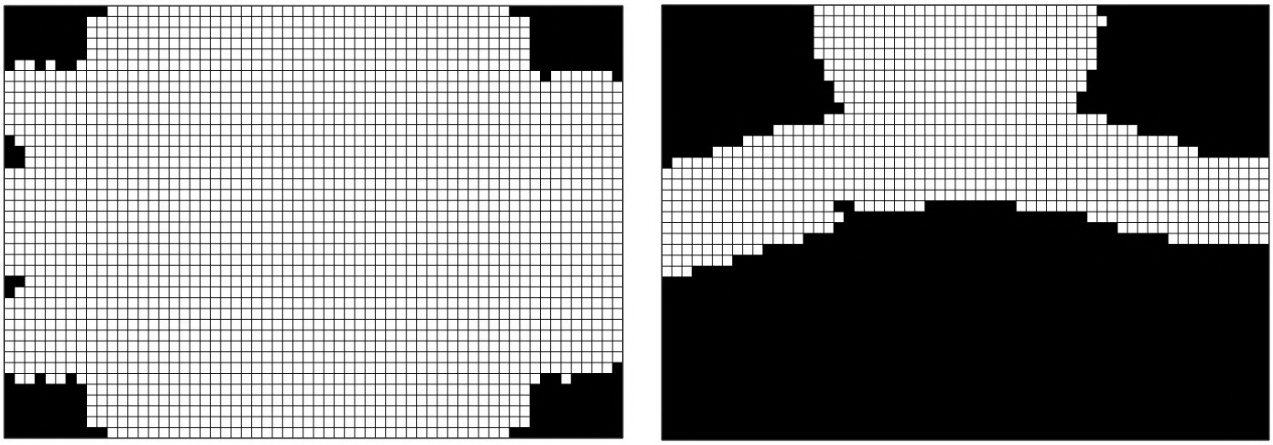

(a) (b)

Figure 14. Microchannel geometry for the microprocessor heat sink using Navier-Stokes corrections, the zero relative pressure boundary condition and (a) a uniform heat source distribution (b) a hot-spot based heat source distribution

It can be observed that Fig. 14(a) presents a structure in which most of the domain remains fluid in order to dissipate most of the heat produced along the distributed heat source, while in Fig. 14(b), the obtained geometry is the result of a trade-off relation between minimal pressure drop and heat dissipation only through the hot-spot regions of the heat source distribution.

6. CONCLUSIONS

The presented results clearly indicate that the adoption of the convective term of the Navier-Stokes equations influenced the shape of the microchannels obtained through topology optimization, transforming a convergent-divergent symmetric single channel structure in a separated double channel structure. This means that the convective effects directly affect the pressure drop obtained along the fluid flow, corroborating the necessity of considering these effects in the fluid flow modeling during topology optimization.

The adoption of the Navier-Stokes also introduced a few disturbances to the topology optimization solution process, but in a real life scenario, the complexity associated to the execution of this a structure containing these disturbances would not be justified. However, the adoption of conditioning techniques of geometry smoothing processes could be considered in future studies.

Also, even that the adoption of the Navier-Stokes correction provided a convergent-divergent single channel structure geometry; the obtained geometry was significantly different than the structure obtained using the Brinkman equation, presenting an asymmetrical behavior. The convergent entrance of the channel structure became more convergent, providing space for the divergent exit of the channel structure develop the fluid flow. This behavior is considered as physically consistent due to the existence of convective effects affecting the flow in this configuration.

The adoption of a zero relative pressure boundary condition also modified the geometry obtained through the topology optimization process, resulting in unexpected solutions such as a convergent single channel structure with only one outlet. This is physically consistent, since the absence of the velocity profile boundary condition does not require continuity through both outlets, and evidently a single outlet configuration would represent a smaller pressure drop than the separation of the flow required for the double outlet solution.

Finally, the adoption of a modified heat source distribution containing only the heat source terms close to the hot-spots of this heat source distribution resulted in a physically consistent behavior, since the obtained geometry presented a good trade-off solution between minimal pressure drop and heat dissipation only through the hot-spot regions. Further studies observing additional configurations and real microprocessor heat source distributions could take these observations a step further.

7. REFERENCES

Bakker, A. and Marshall, E.M., 2004. *Computational Fluid Dynamics*. Encyclopedia of Chemical Processing, New York, <http://www.bakker.org/cfm/publications/EncyclopediaPreprint2004.pdf>.

Bar-Cohen, A. and Wang, P., 2009. "On-chip Hot Spot Remediation with Miniaturized Thermoelectric Coolers". *Microgravity Science and Technology*, Vol. 21, pp. 351-359.

Bendsøe, M.P., 1989. "Optimal shape design as a material distribution problem". *Structural Optimization*, Vol. 1 (4), pp. 193-202.

Bendsøe, M.P. and Sigmund, O., 2004. *Topology Optimization – Theory, Methods and Applications*. Heidelberg: Springer Verlag, Berlin, 2nd edition.

Borrvall, T. and Petersson, J., 2003. "Topology optimization of fluids in Stokes flow". *International Journal of Numerical Methods in Fluids*, Vol. 41, pp. 77-107.

De Lima, C.R., Koga, A.A and Silva, E.C.N., 2010. "Microchannel Heat Sink Design Based On Topology Optimization". *Mecánica Computacional* , Vol. 29, pp. 8307-8317.

Donea, J. and Huerta, A., 2003. *Finite Element Methods for Flow Problems*. Wiley, West Sussex, 1st edition.

Elman, H.C., Ramage, A. and Sylvester, D.J., 2007. "Algorithm 866: IFISS: a Matlab toolbox for modelling incompressible flow". In: *ACM Transactions on Mathematical Software (TOMS)*, Vol. 33 (2).

Hamann, H.F., Lacey, J, Weger, A. and Wakil, J., 2006. "Spatially-resolved imaging of microprocessor power (SIMP): Hotspots in microprocessors". In: *Thermal and Thermomechanical Proceedings 10th Intersociety Conference on Phenomena in Electronics Systems: ITHERM 2006*, San Diego, United States.

Haynes, W.M., Lide, D.R and Bruno, T.J., 2016. *CRC handbook of chemistry and physics : a ready-reference book of chemical and physical data*. CRC Press, Boca Raton, 97th edition.

Incropera, F.P., DeWitt, D.P, Bergman, T.L. and Lavine, A.S., 2011. *Fundamentals of Heat and Mass Transfer*. Wiley, Hoboken, 6th edition.

Koga, A.A., 2010. *Projeto de dispositivos de microcanais utilizando o método de otimização topológica*. M. Sc. thesis, Escola Politécnica – Universidade de São Paulo, São Paulo, Brasil.

Koga, A.A., Lopes, E.C.C., Villa Nova, H.F., De Lima, C.R., Silva, E.C.N., 2013. "Development of heat sink device by using topology optimization". *International Journal of Heat and Mass Transfer*, Vol. 64, pp. 759-772.

Liu, J., Wu, L., Fang, X., 2015. "Using Python to Solve the Navier-Stokes Equations - Applications in the Preconditioned Iterative Methods". *Journal of Scientific Research & Reports*, Vol. 7 (3), pp. 207-217.

Nain, P.K.S., Giri, J.M., Sharma, S., Deb, K., 2010. "Multi-objective Performance Optimization of Thermo-Electric Coolers Using Dimensional Structural Parameters". *In: Swarm, Evolutionary, and Memetic Computing: SEMCCO 2010,* vol 6466, Berlin, Germany.

Olesen, L.H., Okkels, F., Bruus, H., 2005. "A high-level programming-language implementation of topology optimization applied to steady-state Navier–Stokes flow". *International Journal of Numerical Methods in Engineering*, Vol. 65, No. 7, pp. 975-1001.

Parry, W.T., 2009. *ASME International Steam Tables for Industrial Use*. American Society of Mechanical Engineers,, New York, 2nd edition.

Sylvester, D.J., Elman, H.C., Ramage, A., 2019. *Incompressible Flow and Iterative Solver Software (IFISS) – Instalation and Software Guide – Version 3.6*. <http://www.maths.manchester.ac.uk/~djs/ifiss/ifiss_guide_3.0.pdf>.

Ur Rehman, M., Vuik, C and Segal, G., 2008. "Numerical Solution Techniques for the Steady Incompressible Navier-Stokes Problem". *In: Proceedings of the World Congress on Engineering – WCE 2008*, Vol. 2, London, United Kingdom.

Versteeg, H.K. and Malakasera, W., 2007. *An Introduction to Computational Fluid Dynamics – The Finite Volume Method*. Pearson Education, London, 2nd edition.

Zinkiewicz, O.C. and Taylor, R.L., 2002. *The Finite Element Method – Vol. 3: Fluid Dynamics*. Butterworth-Heinemann, Oxford, 5th edition.

8. RESPONSIBILITY NOTICE

The authors are the only responsible for the printed material included in this paper.